Simulation of an asymmetric single dielectric barrier plasma actuator

K. P. Singh[a] and Subrata Roy
Computational Plasma Dynamics Laboratory, Mechanical Engineering, Kettering University, Flint, Michigan 48504

(Received 21 December 2004; accepted 7 September 2005; published online 20 October 2005)

Continuity equations governing electron and ion density are solved with Poisson's equation to obtain spatial and temporal profiles of electron density, ion density, and voltage. The motion of electrons and ions results in charge separation and generation of an electrostatic electric field. Electron deposition downstream of the overlap region of the electrode results in formation of a virtual negative electrode that always attracts the charge separation. The value of charge separation $e(n_i-n_e)$ and the force per volume $\mathbf{F}=e(n_i-n_e)\mathbf{E}$ have been obtained near the dielectric surface for the 50th cycle. Domain integration of the force $\mathbf{F}=e(n_i-n_e)\mathbf{E}$ has been obtained for different plasma densities, frequencies, and rf voltage wave forms. The time average of the x force is positive and the y force is negative over the domain; therefore there is an average net force on the plasma in the positive x and negative y directions. This will result in a moving wave of plasma over the dielectric surface in the positive x direction, which can find application in flow control. © *2005 American Institute of Physics*. [DOI: 10.1063/1.2103415]

I. INTRODUCTION

Radio frequency (rf) based dielectric surface discharge at atmospheric pressures is an emerging field of intense scrutiny because of its applications in flow actuation in aerospace and many other areas.[1,2] These actuators use moderate power, have no mechanical components, have a very fast response, and can apply significant forces in a relatively accurate and autolimiting manner.[3] The schematic of an asymmetric single dielectric barrier plasma actuator is shown in Fig. 1. The grounded electrode for this configuration is embedded in an insulator, and a voltage fluctuating with rf is applied to the electrode exposed to the gas. The electric forces generated for a given interelectrode distance and pressure due to a large applied voltage produce a barrier discharge adjacent to the exposed rf electrode that weakly ionizes the surrounding gas. The plasma at this pressure is highly collisional, causing an efficient energy exchange between charged and neutral species. The electric field $\mathbf{E}$ exerts a net force $q\mathbf{E}$ through the space charge (q) separated plasma within the dielectric barrier discharge.[4,5] This microfilamentary discharge sustains an optical glow within a half cycle through many current pulses of nanosecond duration.[6] The plasma can induce air flow up to several meters per second in atmospheric pressure that has experimentally been shown[1,3] and explained with an approximate theory of the paraelectric effect on the flow.[1] The dielectric characteristics, applied voltage, frequency, and the asymmetric configuration of the electrodes control the paraelectric force. The thickness of the exposed electrode affects the thrust produced by these actuators.[2] Another theoretical attempt conjectures that the higher hydrostatic pressure downstream of the electrode induces the near wall jet.[5] However, the proper mechanism due to which the combination of electrodynamic and collisional processes controls the momentum transfer from charge to neutrals is yet to be theoretically resolved.

A high-fidelity force model needs to be derived from first principles through a simulation of the elementary mechanisms that yield the discharge for general designs. Such a model for volume discharge between two insulated electrodes has been given by Roy and Gaitonde.[4] The model was relatively basic but formed the framework of a first-principles-based methodology using a finite element-based one-dimensional multifluid formulation of a plasma sheath for atmospheric conditions. Simulation results were compared with reported rf glow discharge data[7] in partially ionized helium gas between two insulated electrodes.

In previous works by other authors,[1,2,5] continuity equations related to electron and ion density and Poisson's equation have not been solved simultaneously (some profile of an electric field has been assumed), and therefore fail to give a clear and exact idea about spatial and temporal profiles of electron density, ion density, and voltage. Thus, they fail to explain the physics of an asymmetric single dielectric barrier plasma actuator in an exact manner. Recently Roy[8] has solved these equations simultaneously from the first prin-

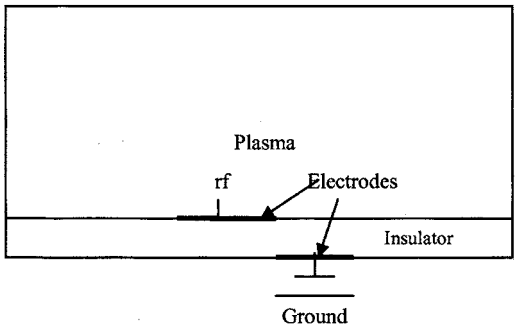

FIG. 1. Schematic of an asymmetric single dielectric barrier plasma actuator.

[a]Electronic mail: ksingh@kettering.edu

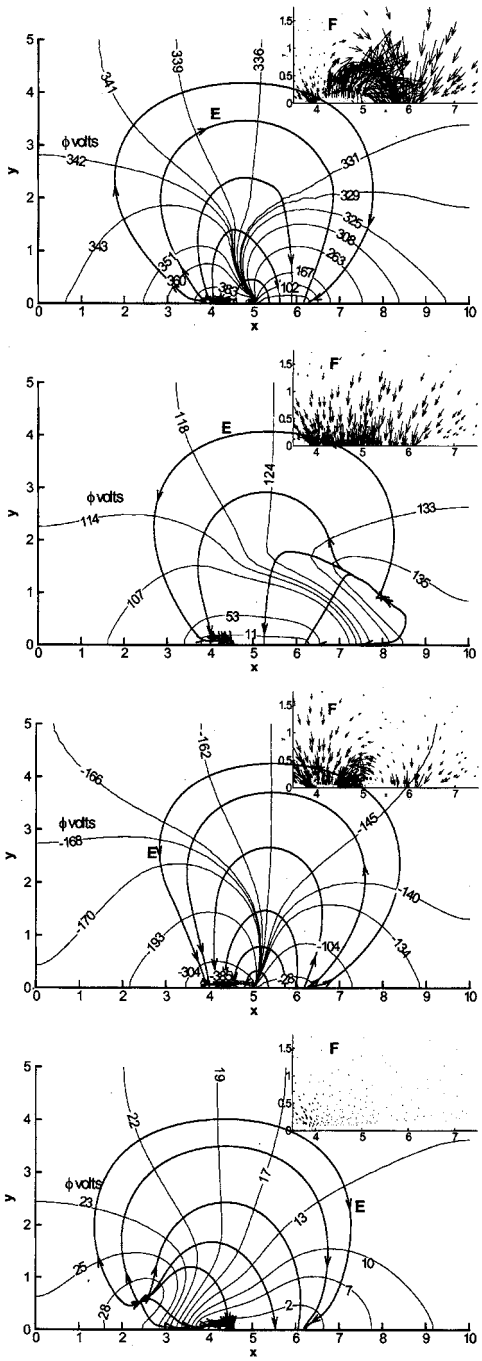

FIG. 2. Contours of voltage distribution with electric field lines overlaid and arrows of the force $\mathbf{F}=(n_i-n_e)\mathbf{E}$ at $\omega t=98.5\pi$, 99π, 99.5π, and 100π.

ciples for an asymmetric single dielectric barrier actuator and demonstrated the effect of the electrohydrodynamic force due to charge separation about the surface on the surrounding neutral gas flow. As a complement to the previous work in this paper, we have explained the physics of an asymmetric single dielectric barrier plasma actuator and studied the effect of different control parameters such as the applied voltage, the rf frequency, and the charge density on the induced force field.

II. GOVERNING EQUATIONS

The dynamics of plasma electrons and ions is governed by following continuity equations and Poisson's equation

$$\frac{\partial n_e}{\partial t}+\nabla\cdot(n_e\mathbf{v}_e)=n_eS, \tag{1}$$

$$\frac{\partial n_i}{\partial t}+\nabla\cdot(n_i\mathbf{v}_i)=n_eS, \tag{2}$$

$$\varepsilon\nabla^2\phi=4\pi e(n_e-n_i), \tag{3}$$

where n_e and n_i, and $\mathbf{v}_e$ and $\mathbf{v}_i$ are electron and ion densities, and velocities, respectively. The Townsend first ionization is determined as

$$s=A\exp[-B/(|E|/p)^{0.4}]p\mu_e|E|s^{-1},$$

$$A=4.4\ \text{cm}^{-1}\ \text{Torr}^{-1}\ \text{and}\ B=14(\text{V/cm Torr})^{0.4};$$

$$n_e\mathbf{v}_e=-n_e\mu_e\mathbf{E}-D_e\nabla\cdot n_e,\ n_i\mathbf{v}_i=-n_i\mu_i\mathbf{E}-D_i\nabla\cdot n_i,$$

$$\mathbf{E}=-\nabla\phi.$$

The electron diffusion is obtained from the Einstein relation, $D_e=(T_e/e)\mu_e$, where T_e is energy in electron volts, e is the elementary charge, ε is the permittivity, and $\mu_e=e/(m_e\nu_{en})$ is the mobility of an electron, where $\nu_{en}\approx10^{12}$/s is the electron-neutral collision frequency. The ion diffusion $D_i=500\ \text{cm}^2/\text{s}$ at 300 K, and the ion mobility μ_i is given by following relation:[9]

$$p\mu_i=(8\times10^3-64|E|/p)\ \text{cm}^2\ \text{V}^{-1}\ \text{s}^{-1}\ \text{Torr}$$
$$\text{for}\ |E|<7500,$$

$$p\mu_i=4.1\times10^4[1-27.44/(|E|/p)^{1.5}]/$$
$$(|E|/p)^{0.5}\ \text{cm}^2\ \text{V}^{-1}\ \text{s}^{-1}\ \text{Torr for}\ |E|\geqslant7500.$$

Charged particle distributions are taken non-Maxwellian and inertia terms are neglected for this highly collisional plasma. The electron temperature is nearly uniform at 1 eV=11, 600 K, and ions and neutrals are in local thermal equilibrium at 300 K. An asymmetric single dielectric barrier plasma actuator finds applications in flow control at low pressure flight conditions in the upper atmosphere; therefore, the working gas, helium, is chosen at a bulk pressure of $p=300$ Torr. Figure 1 shows the schematic of an asymmetric single dielectric barrier plasma actuator. The computational domain is chosen as 10 cm long and 5 cm wide. The lower part of the domain consists of an insulator with dielectric constant $\varepsilon_d=3.5$ (Kapton Polyimide) and thickness 1 mm, and the upper part filled with inert helium gas of $\varepsilon_f=1.0055\varepsilon_0$, where ε_0 is the permittivity of free space. The initial plasma density n_0 is taken as $10^{11}/\text{cm}^3$. The thickness of electrodes is assumed to be infinitesimally small, and lengths of the exposed and insulated electrode are chosen to be 1.27 and 1.2 cm, respectively. The overlap length between electrodes is chosen to be 0.1 mm and the location of the overlap is around $x=5$. A sinusoidal voltage $\phi=\phi_0\sin(2\pi ft)$, where $\phi_0=400$ V, $f=5$ kHz, is applied to the exposed electrode, and the insulated electrode is kept at zero potential as the base of study. The overlap between the electrodes results in dielectric losses at higher voltages; however, at the chosen magnitude it will be negligible. The overlap between the electrodes may

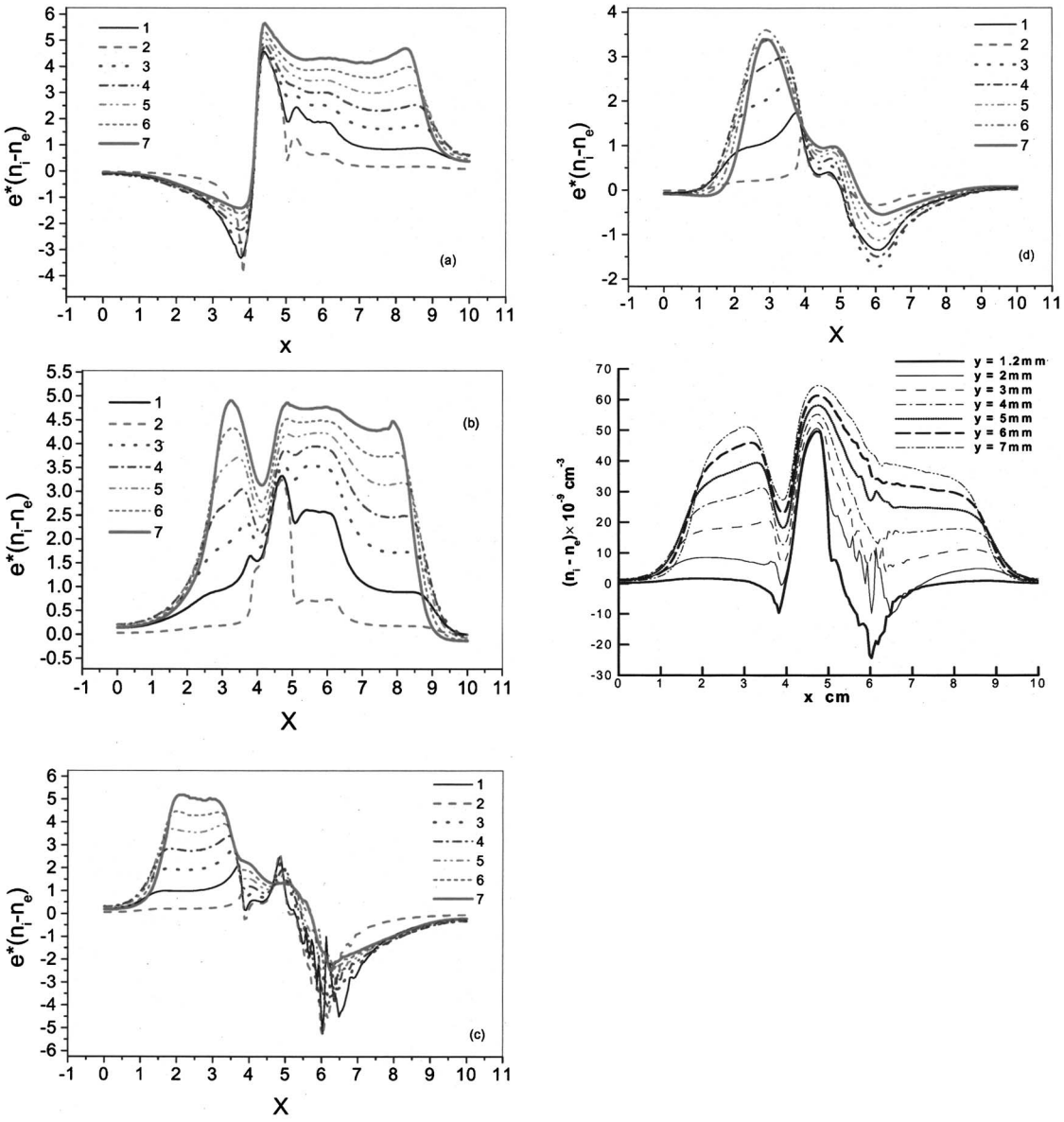

FIG. 3. Charge separation (n_i-n_e) as a function of x for different values of y for $\omega t=98.5\pi$, 99π, 99.5π, and 100π and its time average. Lines 1 to 7 correspond to $y=1.2$, 2, 3, 4, 5, 6, and 7 mm, respectively.

help in the formation of plasma. Different cases have been studied and only changed parameters have been stated. Other parameters remain the same as mentioned above. Equations (1)–(3) are solved for electron and ion density, and the electric potential in the domain, using the finite element method, which is particularly suited for arbitrary geometry and accurate imposition of complicated boundary conditions. The theory and validation details of the method have been archived in earlier papers.[4,10–12] The multiscale issues relevant to the problem are resolved using a 10^{-8} s time step, which is an order of magnitude higher than the dielectric relaxation time 10^{-9} s, but several orders of magnitude smaller than the ion time scale.

III. RESULTS AND DISCUSSION

Figure 2 shows the contours of the voltage and streamlines of the electric field at different points of time during the 50th cycle. These plots are a result of the combined effect of applied rf voltage and electrostatic potential generated due to the charge separation. The inset in the same figure also shows arrows of the force $\mathbf{F}=e(n_i-n_e)\mathbf{E}$. The direction and size of the arrows show the direction of the force and magnitude of the force, respectively. A virtual negative electrode forms downstream the overlap region of the electrodes due to electron deposition, which attracts the charge separation; therefore, the force is directed toward this area.

Figures 3–5 show charge separation $e(n_i-n_e)$, F_x, and F_y as a function of x. Lines 1–7 correspond to $y=1.2$, 2, 3, 4, 5, 6, and 7 mm, respectively. Parts (a)-(d) of each figure are for four points of the 50th cycle at $\omega t=98.5\pi$, 99.0π, 99.5π, and 100π, respectively. Part (e) of each figure is the time average of the quantity during the 50th cycle.

Figure 3 shows the charge separation $e(n_i-n_e)$. The electrons move from the region surrounding grounded electrode towards the edge of the exposed electrode $(x=3.8)$ under the influence of the applied rf voltage until the voltage reaches

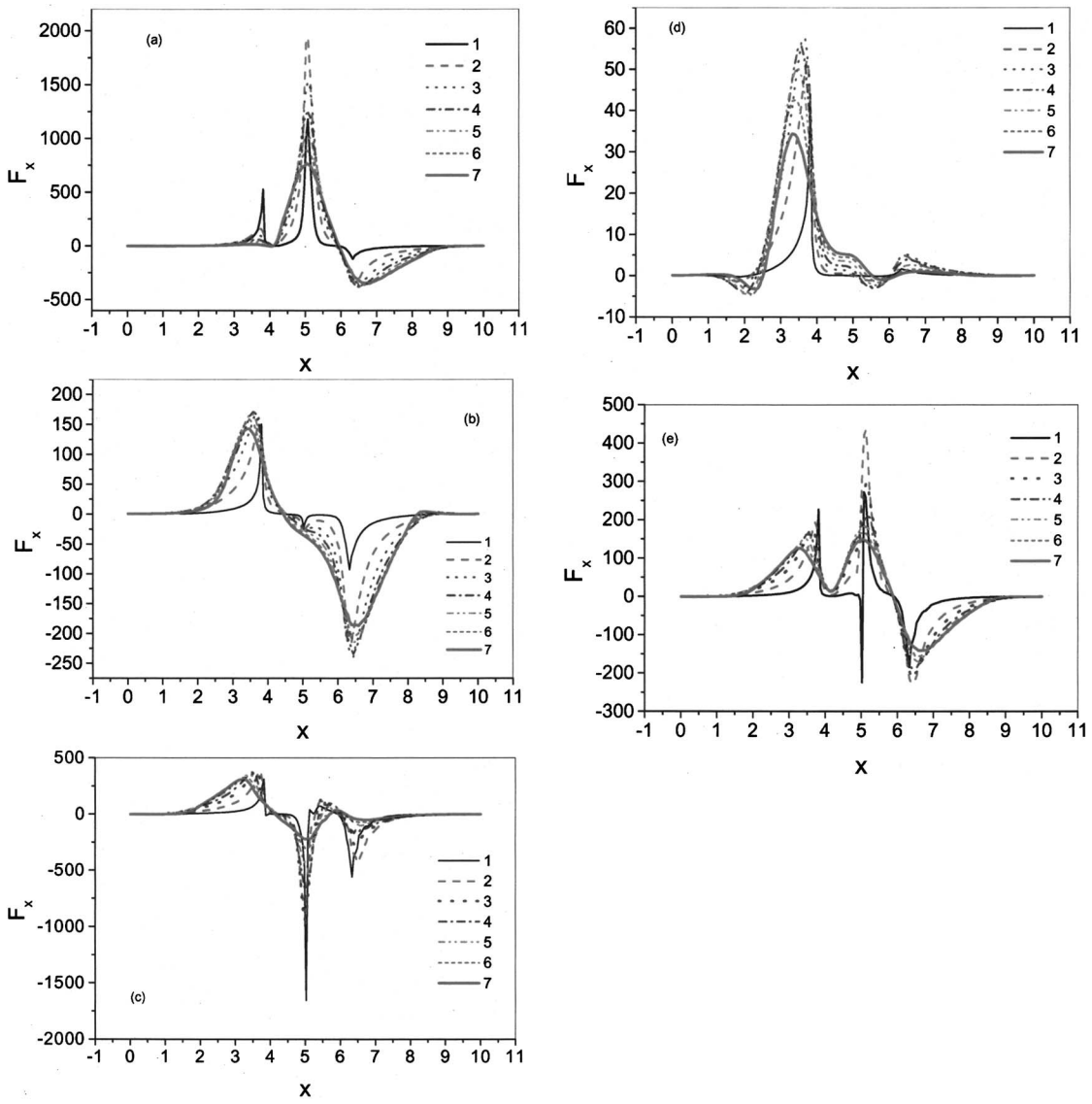

FIG. 4. F_x as a function of x for different values of y for $\omega t=98.5\pi$, 99π, 99.5π, and 100π, and its time average for the same parameters as those in Fig. 3.

its positive peak. The electron density is higher than that of the ion density around $x=3.8$ cm. The electron density is lower than that of ion density over the dielectric surface surrounding grounded electrode. For other cases, the electron density is lower than that of the ion density around $x=3.8$ cm. The electrons move from the region surrounding rf electrode towards the surrounding grounded electrode during the negative part of the cycle. The value of $e(n_i-n_e)$ is negative surrounding grounded electrode in the domain for Figs. 3(c) and 3(d). Figure 3(e) shows the time average of $e(n_i-n_e)$. The time average of $e(n_i-n_e)$ is negative for the region around $x=6$ cm and positive for other regions. The sign and magnitude of $e(n_i-n_e)$ for the different parts of the domain are governed by the direction and magnitude of the electric field and the motion of electrons and ions under this field. When the rf voltage is high, the effect of the electric field due to the applied rf voltage dominates and when the rf voltage is low, the effect of electrostatic field dominates.

Figure 4 shows the x component of the force $\mathbf{F}_x=e(n_i-n_e)\mathbf{E}_x$. The positive peak and negative peak of the force are around the overlap region for $\omega t=98.5\pi$ and $\omega t=99.5\pi$ cases, respectively. For other cases, the positive peak of the force is around $x=3.8$ cm and the negative peak of the force is around $x=6.27$ cm. The magnitude of the force peaks for $y=2$ line in general. For $\omega t=98.5\pi$ and $\omega t=100\pi$ cases, the magnitude of the positive force is higher than that of negative force, and for other cases it is opposite of this. The value of the negative force decreases sharply with the increase in y for $\omega t=100\pi$.

Figure 5 shows the y component of the force $\mathbf{F}_y=e(n_i-n_e)\mathbf{E}_y$. The positive peak of the force is around the overlap region for the $\omega t=98.5\pi$ case and around $x=6$ cm for the $\omega t=100\pi$ case. The magnitude of the force is very small for the latter. The negative peak of the force is around $x=6$ for $\omega t=99\pi$ and around the overlap region for other cases. It is a maximum for the $y=1.2$ mm line, which means it is maximum close to dielectric surface. The magnitude of the negative force decreases sharply with the increase in y for $\omega t=100\pi$ case. Figure 5(e) shows the time average of the force. It can be seen that the average force works only from

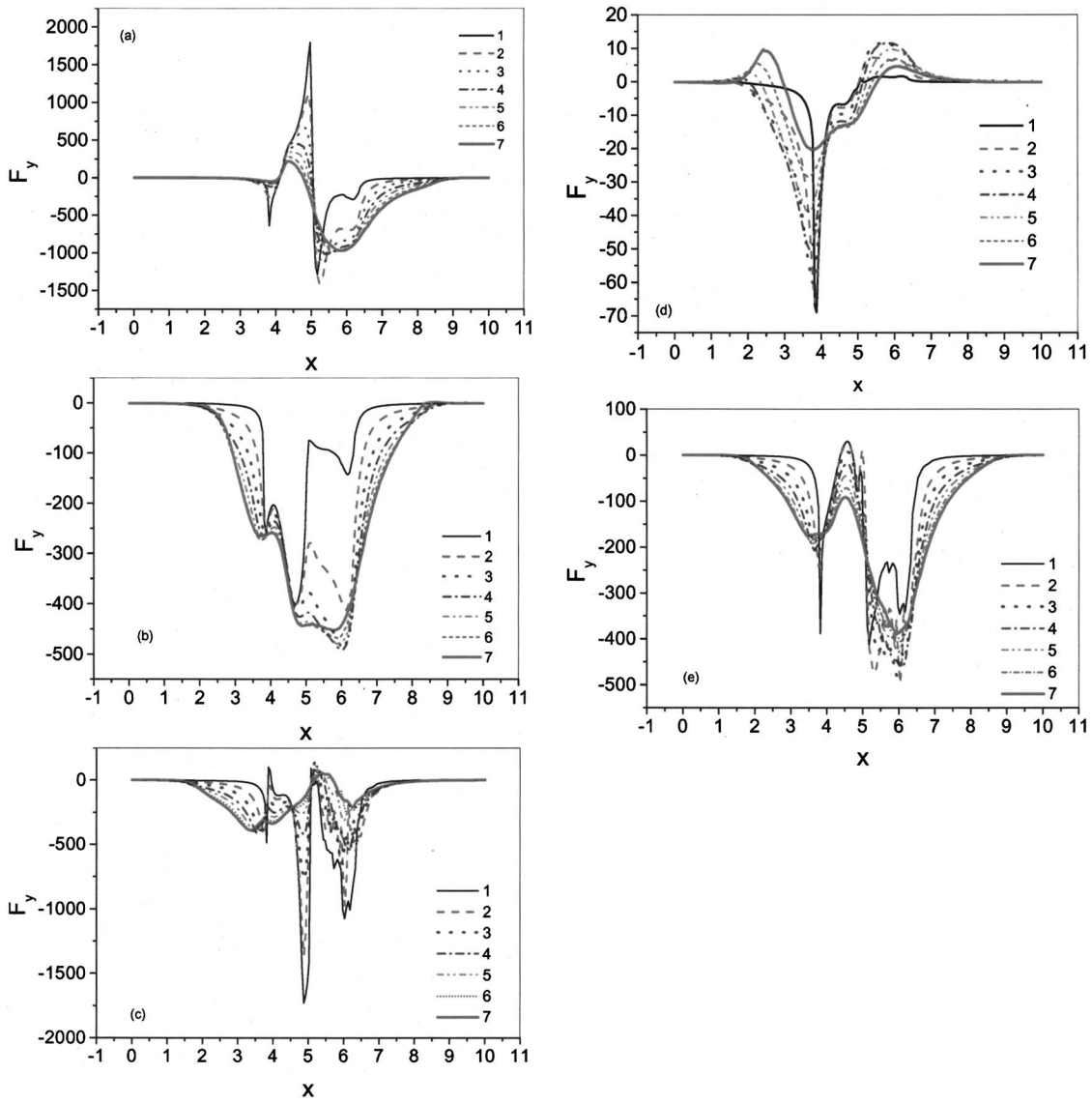

FIG. 5. F_y as a function of x for different values of y for $\omega t=98.5\pi$, 99π, 99.5π, and 100π, and its time average for the same parameters as those in Fig. 3.

$x=3.8$ cm to $x=6.3$ cm and its value is negative except around $x=4.5$, where its value approaches nearly zero.

Figure 6(a) shows domain integration of the x component of the force per cm^2 $e(n_i-n_e)E_x$ as a function of normalized time for the 48th to 50th cycles for 300, 400, and 500 V, and initial plasma density $n_0=10^{10}/\text{cm}^3$. The electron deposition downstream of the rf electrode is small and the generated electrostatic field is also small for the low density case. Therefore, for the $n_0=10^{10}/\text{cm}^3$ case, the force follows the rf voltage. It is positive for the positive part of the cycle and negative for the negative part of the cycle. For other cases, the force is positive for all times except from $\omega t=98.8\pi$ to $\omega t=99.2\pi$ and corresponding time points in other cycles. When the cycle changes the sign, the electron deposition is near the rf electrode, not the downstream of the rf electrode. However, as the negative cycle progresses, the electrons get deposited downstream of the rf electrode, the dielectric surface becomes negatively charged and starts behaving as a virtual negative electrode, and the x force again becomes positive. In this we see that the x force remains positive for most of cycle and over a large time scale, only a positive force will be seen. While the magnitude of the force—both negative and positive—increases with the increase in the magnitude of rf voltage, the negative values are much smaller that the positive x component in any cycle. The time average of the force is 1.76, 1.75, 1.68, and 0.017 dyn/cm^3, respectively, for different cases over the cycles. The time average of the force in low density case is 100 times lower that of the reference case, which is due to a 10-times decrease in both charge separation and electrostatic field. With the increase in voltage effect of the electric field due to applied rf voltage slightly increases so time average of the x force slightly decreases with voltage. Figure 6(b) shows a domain integration of the x component of the force per cm^2 $e(n_i-n_e)E_x$ as a function of normalized time for the 48th to 50th cycle for 1 kHz, 25 kHz, $\phi=\phi_0 \sin^2(\omega t)$, and sawtooth wave form. For the sawtooth wave form, the rf voltage varies from 0 to 800 V. For the 1-kHz case the force follows the rf voltage and it is approximately positive for the positive part of the cycle and negative for the negative part of the

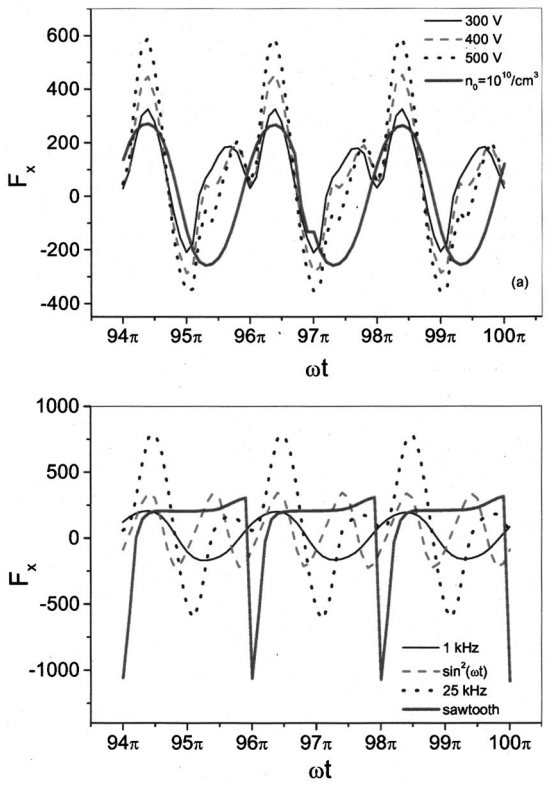

FIG. 6. Domain integration of force F_x (dyn) as a function of normalized time from the 47th to the 50th cycles.

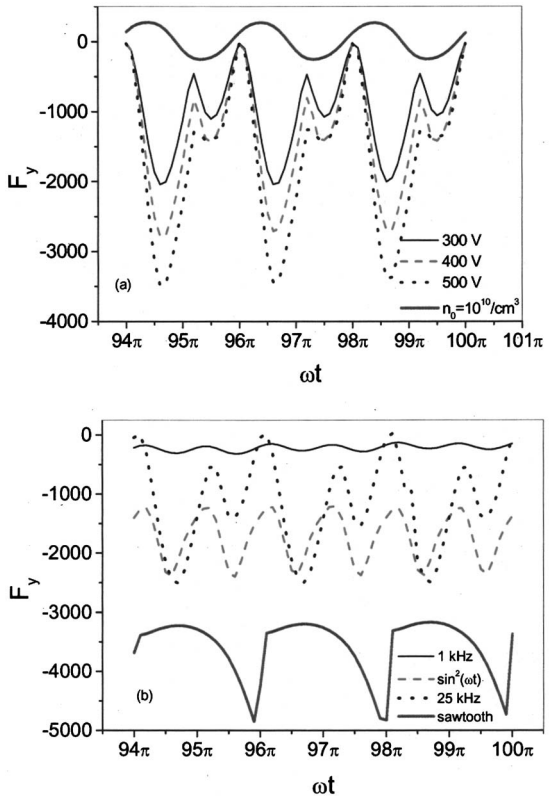

FIG. 7. Domain integration of forces F_y (dyne) as a function of normalized time from the 47th to the 50th cycles.

cycle. For $\phi=\phi_0 \sin^2(\omega t)$ case, the force is negative when the voltage falls after attaining its peak. The electrons get deposited near the rf electrode during increasing voltage and when the voltage starts falling the area around the rf electrode behaves as a cathode and the m force is negative. The magnitude of the force increases with the increase in the frequency of the rf voltage, as can be seen from the 25-kHz case. The effect of the electrostatic field becomes more prominent with the increase in frequency. The E_x is positive and the force is positive for the sawtooth wave profile, except around the point of time when the voltage falls from 800 to 0 V. The time average of the force is 0.34, 1.18, 2.25, and 1.7 dyn/cm^3, respectively, for different cases over the cycles.

Figure 7(a) shows the domain integration of the y component of the force per cm^2 $e(n_i-n_e)E_y$ as a function of normalized time for the 48th to 50th cycles for 300, 400, and 500 V, and initial plasma density 10^{10}/cm^2. For the $n_0=10^{10}$/cm^3 case, the force follows the rf voltage and it is generally positive for the positive part of the cycle and negative for the negative part of the cycle. For other cases, the force is negative for all the time. The dielectric surface becomes negatively charged and behaves as a virtual negative electrode; therefore, E_y is directed towards the dielectric surface. The negative force peaks when the rf voltage is around its positive peak as E_y is strong at this time. With the increase in the magnitude of the rf voltage, the negative magnitude of E_y increases and the negative magnitude of the force also increases. The time average of the force is 19.6, 27.1, 33.36, and 0.13 dyn/cm^3 over the cycles. Figure 7(b) shows the domain integration of the y component of the specific force $e(n_i-n_e)E_y$ as a function of normalized time for the 48th to 50th cycles for 1 kHz (25 kHz and 300 V), $\phi=\phi_0 \sin^2(\omega t)$, and the sawtooth wave profile. For the 1-kHz case the force follows the rf voltage and it is positive for the positive part of the cycle and negative for the negative part of the cycle. The particles have sufficient time to respond to the applied rf voltage and the effect of electrostatic do not dominate. For the $\phi=\phi_0 \sin^2(\omega t)$ case, the largest magnitude of the negative force is approximately equal to that for 400 V case only. It is also equal to the (25 kHz and 300 V) case due to the increase in the force with frequency in the latter case. The magnitude of the negative force is largest in the case of the sawtooth wave profile because peak voltage is 800 V and remains positive for the full cycle in this case. The largest negative force is when the rf voltage is at its positive peak in this case also. The time average of the force is 4.36, −34.40, −23.26, and 71.72 dyn/cm^3, respectively, for different cases over the cycles.

IV. CONCLUSIONS

The spatial and temporal profiles of electron density, ion density, and voltage have been obtained. The electrons and ions move in response to applied rf voltage, with the response of ions being delayed as compared to that of electrons. This results in charge separation and generation of an electrostatic field. The force is positive over the domain during the positive part of the cycle because of the obvious reason that the electric field is towards the positive direction. During the negative part of the cycle, electrons get deposited over the dielectric surface surrounding the grounded electrode, and the dielectric surface starts working as a virtual

negative electrode and the effect of grounded electrode gets cut off. The force is negative only when the voltage changes sign because there is not sufficient deposition of the electrons over the dielectric surface. The time average value of force per unit area in an x direction is positive and in a y direction is negative, which implies that there is an average net electric body force on the plasma in the positive x and negative y directions. This will result in a moving wave of plasma over the dielectric surface in the direction of positive x attenuating faster outside the electrode arrangement. This will be significant for flow control and other relevant applications.

ACKNOWLEDGMENTS

The authors were partially supported by Air Force Research Laboratory Contract No. F33615-98-D-3210 and the AFOSR Grant No. FA9550-05-1-0074 under tasks monitored by Dr. John Schmisseur. The authors acknowledge many thoughtful discussions with Dr. Datta Gaitonde, Professor Natalia Sternberg, and Haribalan Kumar.

[1] J. R. Roth, Phys. Plasmas **10**, 2117 (2003).
[2] C. L. Enloe, T. E. McLaughlin, R. D. VanDyken, K. D. Kachner, E. J. Jumper, and T. C. Corke, AIAA J. **42**, 595 (2004).
[3] T. C. Corke, E. J. Jumper, M. L. Post, D. Orlov, and T. E. McLaughlin, 40th AIAA Aerospace Sciences Meeting, Paper No. 2002-0350 (2002).
[4] S. Roy and D. Gaitonde, J. Appl. Phys. **96**, 2476 (2004).
[5] W. Shyy, B. Jayaraman, and A. Andersson, J. Appl. Phys. **92**, 6434 (2002).
[6] A. Bogaerts, E. Neyts, R. Gijbels, and J. van der Mullen, Spectrochim. Acta, Part B **57**, 609 (2002).
[7] F. Massines, A. Rabehi, P. Decomps, R. B. Gadri, P. Ségur, and C. Mayoux, J. Appl. Phys. **83**, 2950 (1998).
[8] S. Roy, Appl. Phys. Lett. **86**, 101502 (2005).
[9] L. Ward, J. Appl. Phys. **33**, 2789 (1962).
[10] D. Balagangadhar and S. Roy, Comput. Methods Appl. Mech. Eng. **190**, 5465 (2001).
[11] S. Roy and B. P. Pandey, Phys. Plasmas **9**, 4052 (2002).
[12] S. Roy and B. P. Pandey, J. Propul. Power **19**, 964 (2003).